



1

2

3

4

5 **Particle export fluxes to the oxygen minimum zone of the**

6 **Eastern Tropical North Atlantic**

7

8

9

10 Anja Engel<sup>1</sup>, Hannes Wagner<sup>1</sup>, Frédéric A. C. Le Moigne<sup>1</sup>, Samuel T. Wilson<sup>2</sup>

11

12 <sup>1</sup> GEOMAR Helmholtz Centre for Ocean Research Kiel,  
13 24105 Kiel, Germany

14  
15 <sup>2</sup> Daniel K. Inouye Center for Microbial Oceanography: Research and Education, Department  
16 of Oceanography, University of Hawaii, Honolulu, HI 96822, USA

17

18

19

20 *Correspondence to:* Anja Engel (aengel@geomar.de)

21

22

23

24

25

26

27



28 **Abstract.** In the ocean, sinking of particulate organic matter (POM) drives carbon export  
29 from the euphotic zone and supplies nutrition to mesopelagic communities, the feeding and  
30 degradation activities of which in turn lead to export flux attenuation. Oxygen minimum  
31 zones (OMZs) with suboxic water layers ( $<5 \mu\text{mol O}_2 \text{ kg}^{-1}$ ) show a lower carbon flux  
32 attenuation compared to well oxygenated waters ( $>100 \mu\text{mol O}_2 \text{ kg}^{-1}$ ), supposedly due to  
33 reduced heterotrophic activity. This study focuses on sinking particle fluxes through hypoxic  
34 mesopelagic waters ( $<60\% \mu\text{mol O}_2 \text{ kg}^{-1}$ ); these represent  $\sim 100$ -times more ocean volume  
35 globally compared to suboxic waters, but have less been studied. Particle export fluxes and  
36 attenuation coefficients were determined in the Eastern Tropical North Atlantic (ETNA) using  
37 two surface tethered drifting sediment trap arrays with 7 trapping depths located between 100  
38 and 600 m. Data on particulate matter fluxes were fitted to the normalized power function  
39  $F_z = F_{100} (z/100)^{-b}$ , with  $F_{100}$  being the flux at a depth ( $z$ ) of 100m and  $b$  being the attenuation  
40 coefficient. Higher  $b$ -values suggest stronger flux attenuation and are influenced by factors  
41 such as faster degradation at higher temperatures. In this study,  $b$ -values of organic carbon  
42 fluxes varied between 0.74 and 0.80 and were in the intermediate range of previous reports,  
43 but lower than expected from seawater temperatures within the upper 500m. During this  
44 study, highest  $b$ -values were determined for fluxes of particulate hydrolysable amino acids  
45 (PHAA), followed by particulate organic phosphorus (POP), nitrogen (PN), carbon (POC),  
46 chlorophyll  $a$ , and transparent exopolymer particles (TEP), pointing to a sequential  
47 degradation of organic matter components during sinking. Our study suggests that in addition  
48 to oxygen concentration, organic matter composition co-determines transfer efficiency  
49 through the mesopelagial. The magnitude of future carbon export fluxes may therefore also  
50 depend on how organic matter quality in the surface ocean changes under influence of  
51 warming, acidification, and enhanced stratification.

52

53



## 54 1. Introduction

55

56 The biological carbon pump, defined as the export of biologically fixed CO<sub>2</sub> from the surface  
57 to the deeper ocean mainly in the form of sinking particles (Volk and Hoffert, 1985)  
58 influences atmospheric CO<sub>2</sub> concentration and affects ecosystem structure and elemental  
59 distributions in the ocean. The total amount of carbon export as well as the efficiency of the  
60 biological carbon pump, *i.e.* the ratio between export and primary production, are highly  
61 dynamic (Buesseler and Boyd, 2009; Lam et al., 2011). Changes in the efficiency of the  
62 biological carbon pump may have been responsible for past atmospheric CO<sub>2</sub> variability  
63 between glacial-interglacial transition periods (Kohfeld and Ridgwell, 2009) and play a key  
64 role for future climate predictions (Heinze et al., 2015).

65 Most of the POM being exported below the surface mixed layer (<200m in general) is  
66 solubilized and remineralized within the mesopelagic layer, *i.e.* between depths of 200 and  
67 1000 m (Bishop et al., 1978; Suess, 1980). The shallower the carbon remineralization depth,  
68 the more likely is CO<sub>2</sub> to exchange with the atmosphere, and hence drive a shorter carbon  
69 storage time in the ocean (Volk and Hoffert, 1985; Kwon et al., 2009). Factors driving export  
70 flux attenuation in the mesopelagic have therefore a large influence on CO<sub>2</sub> sequestration in  
71 the ocean. The vertical profile of sinking particulate organic carbon (POC) flux has often been  
72 described by a normalized power function:  $F_z = F_{100}(z/100)^{-b}$ , where  $F_z$  is the particle flux as a  
73 function of depth  $z$ ,  $F_{100}$  is the flux at 100 m depth, and  $b$  is the flux attenuation coefficient  
74 (Martin et al., 1987; hereafter *M87*). The authors of the *M87* study derived an ‘open ocean  
75 composite’ for POC export fluxes from North Pacific data with a  $F_{100} = 50.3 \text{ mg m}^{-2} \text{ d}^{-1}$  and  $b$   
76  $= 0.86$ . However strong regional variations of both total export POC fluxes and  $b$  values are  
77 observed (Martin et al., 1987; Buesseler et al., 2007; Torres Valdes et al., 2014; Marsay et al.,  
78 2015) with several factors proposed to control export flux attenuation. Increased attenuation,  
79 *i.e.* higher  $b$ -values, have been related to increased temperature (Marsay et al., 2015),



80 zooplankton feeding activity (Lampitt et al., 1990), coprophagy, coprorhexy, and coprochaly  
81 (Belcher et al. 2016), microbial cycling (Giering et al., 2014) and lack of ballast (LeMoigne et  
82 al., 2012). Decreased flux attenuation, *i.e.* lower  $b$ -values, and thus higher transfer efficiencies  
83 ( $T_{\text{eff}}$ ) have been associated to high particle sinking velocity depending on plankton  
84 community composition, especially the presence of larger phytoplankton cells (Buesseler,  
85 1998; Buesseler and Boyd 2009), particle aggregates (Alldredge and Gotschalk, 1989), and  
86 fecal pellets (Cavan et al., 2015). Organic polymers, such as transparent exopolymer particles  
87 (TEP) increase the rate of aggregate formation due to their high stickiness (Alldredge et al.,  
88 1993; Engel, 2000; Passow, 2002; Chow et al., 2015) and supposedly play an important role  
89 in particle export fluxes (Passow, 2002; Arrigo, 2007; Chow et al., 2015). TEP are carbon-  
90 rich particles that form from dissolved polysaccharides (Engel et al., 2004). When included in  
91 sinking POM inventories, TEP may increase carbon relative to nitrogen export fluxes, a  
92 mechanism potentially counteracting rising CO<sub>2</sub> concentration in the atmosphere (Schneider  
93 et al., 2004; Arrigo, 2007; Engel et al., 2014). However, TEP themselves are non-sinking due  
94 to a high water content and low density (Azetzu-Scott and Passow, 2004), and little  
95 quantitative data are available on TEP export by sinking particles so far (Passow et al., 2000;  
96 Martin et al., 2011; Ebersbach et al., 2014). Thus, the role of TEP in carbon export is still  
97 unresolved.

98 Reduced POC flux attenuation has also be suggested for oxygen minimum zones (OMZs)  
99 (Martin et al., 1987; Haake et al., 1992; Devol and Hartnett, 2001; Van Mooy et al., 2002;  
100 Keil et al., 2015) as a consequence of reduced zooplankton feeding and microbial degradation  
101 activities in suboxic ( $<5 \mu\text{mol O}_2 \text{ kg}^{-1}$ ) waters. So far, the vast majority of mesopelagic  
102 downward POM flux measurements originate from well oxygenated waters ( $>100 \mu\text{mol O}_2$   
103  $\text{kg}^{-1}$ ). In the *M87* study, five sets of drifting sediment traps were deployed in the oxygenated  
104 North Pacific and four sets were deployed in the Eastern Tropical North Pacific (ETNP)  
105 OMZ. The flux attenuation coefficients ( $b$ ) for the oxygenated North Pacific averaged  $0.90 \pm$



106 0.06, while lower  $b$  values averaging  $0.66 \pm 0.24$  were measured in the ETNP OMZ. In  
107 agreement, Devol and Hartnett (2001) and Van Mooy et al. (2002) observed low particle  
108 attenuation in the OMZ of the ETNP off Mexico, yielding  $b$  coefficients of 0.36 and 0.40,  
109 respectively. Keil et al. (2015) found  $b$  values of 0.59-0.63 in the suboxic Arabian Sea. These  
110 studies thus indicate that a greater proportion of the sinking POM escapes degradation while  
111 sinking through suboxic waters. However, influence of oxygen on organic matter degradation  
112 may vary between individual components. For instance, degradation of hydrolysable amino  
113 acid under suboxic conditions was found to continue with the same rate as compared to oxic  
114 conditions (Van Mooy et al. 2002; Pantoja et al. 2004), suggesting that anaerobic and micro-  
115 aerobic bacteria preferentially utilize nitrogen-rich components.

116

117 So far, little is known on sinking POM flux attenuation in hypoxic waters ( $<60 \mu\text{mol O}_2 \text{ kg}^{-1}$ ),  
118 which are more widespread (~4% of ocean volume) compared to suboxic waters ( $< 0.05\%$  of  
119 ocean volume). Laboratory studies indicated that particle aggregates sinking through hypoxic  
120 waters can become suboxic within their interior due to oxygen diffusion limitation and evolve  
121 microbial degradation processes typical for suboxic waters (Alldredge and Cohen, 1987;  
122 Ploug et al., 1997; Stief et al., 2016). For example, at an ambient  $\text{O}_2$  concentration of  $60 \mu\text{mol}$   
123  $\text{kg}^{-1}$ , the  $\text{O}_2$  uptake by a 2 mm (diameter) aggregate was diffusion-limited and a 0.5 mm wide  
124 anoxic core occurred within its interior (Ploug and Bergkvist, 2015). Since OMZs are  
125 expected to expand in the future as a consequence of global warming and altered circulation  
126 patterns (Stramma et al., 2008), the role of oxygen in controlling the biological pump  
127 efficiency needs to be better constrained for predicting ocean-climate feedbacks. In order to  
128 assess what controls carbon flux attenuation and depth-related changes in sinking particle  
129 composition in hypoxic waters, we determined downward POM fluxes in the ETNA off the  
130 coast of Mauretania, which exhibits an extensive hypoxic OMZ between 300 and 500 m. We  
131 used two parallel drifting surface-tethered drifting sediment trap devices with particle



132 interceptor traps (PITs) at 7-8 different depths between 60-600 m to estimate fluxes to and  
133 within the OMZ.

134

135

## 136 2. Methods

### 137 2.1. The Study area

138 The study was conducted from March 17<sup>th</sup> to April 16<sup>th</sup> 2014 during a cruise of the RV  
139 METEOR to the ETNA region off the coast of Mauretania (Fig. 1a). The study area included  
140 hypoxic waters with minimum values of oxygen concentration of 40  $\mu\text{mol kg}^{-1}$  as determined  
141 by CTD (Seabird) casts with two calibrated oxygen sensors at midwater depths of 350-500 m  
142 (Fig. 1b) (Visbeck, 2014).

143

### 144 2.2. Sediment trap operation and sample analysis

145 Free-drifting surface tethered sediment trap devices were deployed for 196 h during the first  
146 deployment and 281h during the second deployment (Fig. 1c). The first trap device was  
147 deployed on the 24<sup>th</sup> of March 2014 (11:00 UTC) at 10.00°N 21.00°W with 12 Particle-  
148 Interceptor-Traps (PITs) at each of 8 depths: 60, 100, 150, 200, 300, 400, 500, and 600 m.  
149 The device was recovered on the 1<sup>st</sup> of April 2014 (14:30 UTC) at 10.46°N 21.39°W. The  
150 second device was deployed on the 27<sup>th</sup> of March 2014 (16:00 UTC) at 10.25°N 21°W with  
151 12 PITs at each of 7 depths: 100, 150, 200, 300, 400, 500, and 600 m. The second trap device  
152 was recovered on the 8<sup>th</sup> of April 2014 (09:00 UTC) at 10.63°N 21.50°W. Both devices  
153 slowly drifted northwest and were recovered approximately 37 nm away from their  
154 deployment location (Fig. 1c). Within the drifting area oxygen concentration in the OMZ  
155 resembled the overall pattern of the Mauretanian upwelling with fully hypoxic conditions  
156 between 300 and 500 m (Fig. 1d).



157 The design of the trap devices and the drifting array basically follows Knauer et al. (1979),  
158 with 12 PITs mounted on a polyvinylchloride (PVC) cross frame. The PITs were acrylic tubes  
159 with an inside diameter of 7 cm, an outside diameter of 7.6 cm and a height of 53 cm, leading  
160 to an aspect ratio of 7.5. The aspect ratio and a baffle system consisting of smaller acrylic  
161 tubes attached to the top end of each PIT help to reduce drag-induced movement within the  
162 trap (Soutar et al., 1977). PVC crosses with PITs were attached to a free-floating line, which  
163 was buoyed at the surface and weighed at the bottom. The surface buoys of the arrays carried  
164 GPS/Iridium devices and flashlights.

165 Prior to each deployment, each PIT was filled with 1.5 L filtered surface seawater (0.2  $\mu\text{m}$   
166 pore size cartridge) collected from the ship's underway seawater system, up to 3/4 of the  
167 PITs' height. A brine solution was prepared by dissolving 50 g L<sup>-1</sup> sodium chloride with  
168 filtered surface seawater and subsequently filtered through a 0.2  $\mu\text{m}$  cartridge to remove  
169 excess particulates. 20 ml of formalin was then added per L of the solution to achieve a brine  
170 solution with 2% formalin. The preservative solution was then slowly transferred into each  
171 PIT beneath the 1.5 L of filtered seawater using a peristaltic pump. PITs were covered with  
172 lids immediately, to minimize contamination before deployment.

173 Sample treatment after trap recovery followed recommendations given by Buesseler et al.  
174 (2007). After recovery, all PITs were capped to minimize contamination. The density gradient  
175 was visually inspected and found intact at the position of prior to deployment or at a  
176 maximum 2 cm above. Then, seawater was pumped out of each PIT using a peristaltic pump  
177 down to 2-3 cm above the density gradient. The remaining ~0.6 L were subsequently  
178 transferred to canisters, pooled from 11 tubes per depth. 40 ml formalin were added to each  
179 canister. Samples from each depth were passed through a 500  $\mu\text{m}$  nylon mesh. Swimmers  
180 were removed from the mesh with forceps under a binocular microscope and the remaining  
181 particles, which stuck to the mesh, were transferred back to the sample. Samples were  
182 subsequently split into aliquots of the total sample. Therefore, the pooled sample was



183 transferred into a round 10 L canister and stirred at medium velocity with a magnetic bar.  
184 Aliquots were transferred into 0.5 L Nalgene bottles with a flexible tube using a peristaltic  
185 pump. Aliquots samples were filtered under low pressure (<200 mbar) onto different filter  
186 types (combusted GF/F 0.7  $\mu\text{m}$ , polycarbonate 0.4  $\mu\text{m}$ , or cellulose acetate 0.8  $\mu\text{m}$ ; see below)  
187 for different analyses and stored frozen (-20 °C) until analyses.

188

#### 189 2.2.1. Biogeochemical Analyses

190 The following parameters were determined: Total particulate mass (TPM), particulate organic  
191 carbon (POC), particulate nitrogen (PN), particulate organic phosphorus (POP), biogenic  
192 silica (BSi), chlorophyll *a* (Chl *a*), particulate hydrolysable amino acids (PHAA) and  
193 transparent exopolymer particles (TEP).

194

195 TPM was analyzed in triplicate. The following aliquots were filtered in triplicate onto pre-  
196 weighed 0.4  $\mu\text{m}$  polycarbonate filters: 800 ml (2 x 400 ml; 8 % of total sample) for the depths  
197 of 600 m to 300 m of deployment #1, 400 ml (4 % of total sample) for the depths of 200 m  
198 and 150 m of deployment #1 and for all depths of deployment #2, 420 ml (4 % of total  
199 sample) for the depth of 100 m and 60 m of deployment #1. Filters were rinsed two times  
200 with Milli-Q water, dried at 60°C for 4 h and stored until weight measurement on a Mettler  
201 Toledo XP2U microbalance.

202

203 POC and PN aliquots were filtered in triplicate onto combusted (8h at 500°C) GF/F filters  
204 (Whatmann, 25 mm): 400 ml (4 % of total sample) for the depths of 600 m to 150 m of  
205 deployment #1, 420 ml (4 % of total sample) for the depths of 100 m and 60 m of deployment  
206 #1, 100 ml (1 % of total sample) for all depths of deployment #2. For the depths of 150 m,  
207 100 m and 60 m of deployment #1, 400 - 420 ml (4 % of total sample) was filtered onto two  
208 filters, due to the high particle load at these depths. Filters were exposed to fuming



209 hydrochloric acid in a fuming box over night to remove carbonate and subsequently dried  
210 (60°C, 12 h). For analysis, the filters were wrapped in tin foil and analysed using an Euro EA  
211 elemental analyzer calibrated with an acetanilide standard. For the depths of 150, 100 and 60  
212 m of deployment #1 the sum of both filters was taken.

213

214 POP was determined in triplicate, except for 60 m depth of deployment #1, which was only  
215 determined in duplicate. The following aliquots were filtered in onto combusted GF/F filters  
216 (Whatmann, 25 mm): 400 ml (4 % of total sample) for the depths of 600 m to 150 m of  
217 deployment #1, 420 ml (4 % of total sample) for the depths of 100 m and 60 m of deployment  
218 #1, 100 ml (1 % of total sample) for all depths of deployment #2. For the depths of 200 m to  
219 60 m of deployment #1, the volume of 400 ml/ 420 ml (4 % of total sample) was filtered onto  
220 two filters, due to the high particle load at these shallower depths. Organic phosphorus  
221 collected on the filters was digested in the potassium peroxydisulphate containing substance  
222 Oxisolv (Merck) for 30 min in a pressure cooker and measured colorimetrically as ortho-  
223 phosphate following the method of Hansen and Koroleff (1999).

224

225 PHAA were determined in duplicate. The following aliquots were filtered onto combusted  
226 GF/F filters (25 mm): 400 ml (4 % of total sample) for the depths of 600 m to 150 m of  
227 deployment #1, 420 ml (4 % of total sample) for the depths of 100 m and 60 m of deployment  
228 #1, 100 ml (1 % of total sample) for all depths of deployment #2. For the depths of 150 m,  
229 100 m and 60 m of deployment #1, the volume of 400 ml / 420 ml (4 % of total sample) was  
230 filtered onto two filters, due to the high particle load at these shallower depths. PHAA  
231 analysis was performed according to Lindroth & Mopper (1979) and Dittmar et al. (2009)  
232 with some modifications. Duplicate samples were hydrolyzed for 20 h at 100°C with  
233 hydrochloric acid (30%, Suprapur, Merck) and neutralized by acid evaporation under vacuum  
234 in a microwave at 60°C. Samples were washed with water to remove remaining acid.



235 Analysis was performed on a 1260 HPLC system (Agilent). Thirteen different amino acids  
236 were separated with a C18 column (Phenomenex Kinetex, 2.6  $\mu\text{m}$ , 150 x 4.6 mm) after in-line  
237 derivatization with o-phthalaldehyde and mercaptoethanol. The following standard amino  
238 acids were used: aspartic acid (AsX), glutamic acid (GIX), histidine (His), serine (Ser),  
239 arginine (Arg), glycine (Gly), threonine (Thr), alanine (Ala), tyrosine (Tyr), valine (Val),  
240 phenylalanine (Phe), isoleucine (Ileu), leucine (Leu),  $\gamma$ - amino butyric acid (GABA).  $\alpha$ -  
241 amino butyric acid was used as an internal standard to account for losses during handling.  
242 Solvent A was 5% acetonitrile (LiChrosolv, Merck, HPLC gradient grade) in  
243 sodiumdihydrogenphosphate (Merck, suprapur) buffer (pH 7.0), Solvent B was acetonitrile. A  
244 gradient was run from 100% solvent A to 78% solvent A in 50 minutes. The detection limit  
245 for individual amino acids was 2 nmol monomer  $\text{L}^{-1}$ . The precision was <5%, estimated as the  
246 standard deviation of replicate measurements divided by the mean. The degradation index  
247 (DI) was calculated from the amino acid composition following Dauwe et al. (1999).

248

249 BSi was determined in triplicate. The following aliquots were filtered onto cellulose acetate  
250 filters (0.8  $\mu\text{m}$ ): 400 ml (4 % of total sample) for the depths of 600 m to 150 m of deployment  
251 #1, 420 ml (4 % of total sample) for the depths of 100 m and 60 m of deployment #1, 200 ml  
252 (2 x 100 ml; 2 % of total sample) for all depths of deployment #2. Filters were incubated with  
253 25 ml NaOH (0.1 M) at 85°C for 2h 15min in a shaking water bath. After cooling of the  
254 samples, analysis was conducted according to the method for determination of  $\text{Si}(\text{OH})_4$  by  
255 Hansen and Koroleff (1999). Fluxes of biogenic opal were calculated assuming a water  
256 content of ~10% and therefore the chemical formula  $\text{SiO}_2 \times 0.4\text{H}_2\text{O}$  with a density of ~2.1 g  
257  $\text{cm}^{-3}$  (Mortlock and Fröhlich 1989).

258

259 Chl *a* was determined in duplicate. The following aliquots were filtered onto GF/F filters (25  
260 mm): 400 ml (4 % of total sample) for the depths of 600 m to 150 m of deployment #1, 420



261 ml (4 % of total sample) for the depths of 100 m and 60 m of deployment #1, 100 ml (1 % of  
262 total sample) for all depths of deployment #2. For the depths of 200 m to 60 m of deployment  
263 #1, the volume of 400 ml / 420 ml (4 % of total sample) was filtered onto two filters, due to  
264 the high particle load at these shallower depths. Samples were analyzed after extraction with  
265 10ml of acetone (90%) on a Turner fluorimeter after Welschmeyer (1994). Calibration of the  
266 instrument was conducted with spinach extract standard (Sigma Aldrich).

267

268 TEP were determined in quadruplet by microscopy after Engel (2009). Between 3.5 and 10 ml  
269 (0.03-0.1% of total sample for the depths of deployment #1 and #2 were filtered onto 0.4 µm  
270 Nuclepore membrane filters (Whatmann) and stained with 1 mL Alcian Blue solution. Filters  
271 were mounted onto Cytoclear© slides and stored at -20 °C until microscopy analysis using a  
272 light microscope (Zeiss Axio Scope A.1) connected to a camera (AxioCAM Mrc). Filters  
273 were screened at 200x magnification. 30 pictures were taken randomly from each filter in two  
274 perpendicular cross sections (15 pictures each; resolution 1040 x 1040 pixel, 8-bit color  
275 depth). Image analysis software WCIF ImageJ (Version 1.44, Public Domain, developed at  
276 the US National Institutes of Health, courtesy of Wayne Rasband, National Institute of Mental  
277 Health, Bethesda, Maryland) was used to semi-automatically analyse particle numbers and  
278 area.

279

280 The carbon content of TEP (TEP-C) was estimated after Mari (1999) using the size dependent  
281 relationship:

282

$$283 \text{ TEP-C} = a \sum_i (n_i r_i^D), \quad (1)$$

284

285 with  $n_i$  being the number of TEP in the size class  $i$  and  $r_i$  the mean equivalent spherical radius  
286 of the size class. The constant  $a = 0.25 * 10^{-6}$  (µg C) and the fractal dimension of aggregates



287 D= 2.55 were proposed by Mari (1999). TEP-C was only calculated for the size fraction <5  
288  $\mu\text{m}$  including mainly free TEP, because larger TEP included TEP covered aggregates with  
289 solid particles. Estimating carbon content of these larger particles would overestimate TEP-C  
290 as the volume of the other particles would be included.

291

### 292 2.3. Calculations and statistics

293 Fluxes of  $\text{CaCO}_3$  and lithogenic matter (lith) were calculated as:

294

$$295 \quad [\text{CaCO}_3 + \text{lith}] = [\text{TPM}] - [\text{POM}] - [\text{Opal}], \quad (2)$$

296

297 Total mineral ballast ( $\text{ballast}_{\text{total}}$ ) was calculated as:

298

$$299 \quad [\text{ballast}_{\text{total}}] = [\text{TPM}] - [\text{POM}], \quad (3)$$

300

301 and the percentage of  $\text{ballast}_{\text{total}}$  ( $\% \text{ballast}_{\text{total}}$ ) was calculated as:

302

$$303 \quad [\% \text{ballast}_{\text{total}}] = ([\text{TPM}] - [\text{POM}]) / [\text{TPM}] * 100, \quad (4)$$

304

305 The transfer efficiency ( $T_{\text{eff}}$ ) of particulate components was calculated as the ratio of fluxes at  
306 600 m to those at 100 m.

307

308 Calculated mean values include replicate measurements of both deployments. Data fits and  
309 statistical tests were performed with the software packages Microsoft Office Excel 2010,  
310 Sigma Plot 12.0 (Systat) and Ocean Data View (ODV) (Schlitzer, 2013). Weighted-average  
311 gridding was used in ODV to display data according to data coverage with automatic scale  
312 lengths. The overall significance level was  $p < 0.05$ .



313

314

315 **3. Results and Discussion**

316

## 317 3.1. Fluxes of different compounds

318 Export fluxes of TPM and particulate organic elements determined during both trap  
319 deployments showed good overall agreement and a decrease with depth, fitting well to the  
320 power law function of *M87* (Fig. 2a-d, Fig.3a-d and Table 1). Averaging fluxes from both  
321 deployments yielded a total mass flux of  $240 \pm 34 \text{ mg m}^{-2} \text{ d}^{-1}$  at 100 m decreasing to  $141 \pm$   
322  $8.8 \text{ mg m}^{-2} \text{ d}^{-1}$  in the core of the OMZ (400 m) (Fig. 2a). Fluxes of POC, PN and POP at 100  
323 m depth were  $73 \pm 8.8$ ,  $13 \pm 1.4$  and  $0.67 \pm 0.06 \text{ mg m}^{-2} \text{ d}^{-1}$ , respectively, and decreased to  $26$   
324  $\pm 4.5$ ,  $3.0 \pm 0.41$  and  $0.19 \pm 0.04 \text{ mg m}^{-2} \text{ d}^{-1}$  at 400 m depth (Fig. 2b-d). The contribution of  
325 POC flux to total mass flux (% OC) decreased from about 30% at 60-150 m depth to 17-20%  
326 at 400 m depth and showed only a minor decrease below 400 m, to 14-16% at 600 m depth.  
327 Similarly, the percentage of PN flux to total mass flux (% N) showed the largest decrease  
328 between 60 and 400 m, i.e. from 6.6% to 2.0-2.3%, and less decline below, reaching 1.7-1.8%  
329 at 600 m. The percentage of POP flux to total mass flux (% P) decreased from 0.37% at 60 m  
330 depth to 0.11-0.16% at 400 m depth, and remained constant below 400 m depth. No previous  
331 data are available for POM export fluxes at our study site for direct comparison. However,  
332 our trap data compare well to carbon export fluxes estimated from particle size data (i.e. 10-  
333  $300 \text{ mg C m}^{-2} \text{ d}^{-1}$ ) reported for 100 m depth in the area off Cape Blanc (Mauritania) by  
334 Iversen et al. (2010).

335

336 Fluxes of phytoplankton biomass, as indicated from Chl *a*, were similar at 100 m during both  
337 deployments, with  $104 \pm 1.5 \text{ } \mu\text{g Chl } a \text{ m}^{-2} \text{ d}^{-1}$  during the first and  $116 \pm 6.2 \text{ } \mu\text{g m}^{-2} \text{ d}^{-1}$  during  
338 the second deployment, but behaved differently below, with a stronger flux attenuation above



339 the OMZ during the first compared to the second deployment (Fig. 3a). Fluxes within the  
340 OMZ core were  $35 \pm 0.1 \mu\text{g m}^{-2} \text{d}^{-1}$  (#1) and  $53 \pm 0.5 \mu\text{g m}^{-2} \text{d}^{-1}$  (#2) respectively.

341

342 Opal fluxes were also similar during both deployments, yielding an average of  $47 \pm 3.6 \text{ mg m}^{-2}$   
343  $\text{d}^{-1}$  at 100 m, steadily decreasing to  $32 \pm 2.4 \text{ mg m}^{-2} \text{d}^{-1}$  at 400 m depth (Fig. 3b). Similar to  
344 Chl *a*, opal fluxes were slightly higher above the OMZ during the second compared to the  
345 first deployment, but quite similar or even lower below the OMZ. This may indicate that the  
346 second trap device, which drifted more northerly (Fig. 1c), exploited waters of a more recent  
347 diatom bloom compared to the first deployment.

348 Fluxes of  $[\text{CaCO}_3 + \text{lith}]$  were similar to opal fluxes during the first deployment ( $F_{100}=52 \text{ mg}$   
349  $\text{m}^{-2} \text{d}^{-1}$ ) but considerably lower during the second ( $F_{100}=14.8 \text{ mg m}^{-2} \text{d}^{-1}$ ) (data not shown).

350

351 During this study, export fluxes of TEP were estimated from decrease over depth of total  
352 particle area and showed the strongest depth attenuation between 60 and 100 m during the  
353 first deployment (Fig. 3c). Like Chl *a* fluxes, TEP export fluxes were slightly higher during  
354 the second compared to the first deployment. At 100 m depth, average TEP flux was  $1860 \pm$   
355  $46 \text{ cm}^2 \text{ m}^{-2} \text{d}^{-1}$  and decreased to  $1190 \pm 52 \text{ cm}^2 \text{ m}^{-2} \text{d}^{-1}$  at 400 m. Using a TEP size to carbon  
356 conversion according to Mari (1999) yielded to an average TEP-C ( $<5 \mu\text{m}$ ) flux of  $1.73 \pm$   
357  $0.35 \text{ mg C m}^{-2} \text{d}^{-1}$  at 100m depth, slightly decreasing to  $1.64 \pm 0.28 \text{ mg m}^{-2} \text{d}^{-1}$  at 400 m and  
358 further to  $0.90 \pm 0.32 \text{ mg m}^{-2} \text{d}^{-1}$  at 600 m. Although TEP supposedly play an important role  
359 in particle export fluxes (Passow, 2002; Arrigo, 2007; Chow et al., 2015), only a few previous  
360 estimates for TEP export fluxes based on sediment traps have been given so far to which we  
361 can compare our data. Martin et al. (2011) measured TEP export fluxes during a spring  
362 bloom in the Iceland Basin (Northeast Atlantic Ocean) using the PELAGRA neutrally  
363 buoyant sediment traps and determined values in the range of 30-120 mg Gum Xanthan  
364 Equivalent  $\text{m}^2 \text{d}^{-1}$ . Ebersbach et al. (2014) obtained lower values of  $\sim 5 \text{ mg Gum Xanthan}$



365 Equivalent  $\text{m}^2 \text{d}^{-1}$  during the LOHAFEX iron fertilization experiment in the Southern Ocean.  
366 Assuming a conversion factor of  $0.063 \text{ C mg}^{-1}$  Gum Xanthan after Engel and Passow (2001)  
367 these previous estimates suggest TEP-C export fluxes of  $0.3 \text{ mg m}^{-2} \text{d}^{-1}$  for the Southern  
368 Ocean and a range of  $1.9\text{--}7.5 \text{ mg m}^{-2} \text{d}^{-1}$  for the North Atlantic spring bloom. Our data on TEP  
369 export fluxes for ETNA region are within the range of both previous studies, but closer to the  
370 lower estimates for the North Atlantic. It has to be emphasized, though, that our calculated  
371 TEP-C fluxes are likely underestimates, since only suspended, i.e. ‘free’ TEP  $< 5 \mu\text{m}$  were  
372 taken into account. TEP-C associated to aggregates cannot be determined with the applied  
373 microscopic technique. Overall, TEP-C export fluxes in the ETNA were significantly related  
374 to Chl *a* fluxes, yielding  $[\text{TEP-C, mg m}^{-2} \text{d}^{-1}] = 11.9 [\text{Chl } a; \text{mg m}^{-2} \text{d}^{-1}] + 0.74$  ( $r^2=0.59$ ,  $n=$   
375  $15$ ,  $p<0.01$ ).

376

377 A strong decrease at shallow depth (60–100 m) was also observed for PHAA fluxes during  
378 the first deployment (Fig. 3d). Average PHAA fluxes were  $330 \pm 51 \mu\text{mol m}^{-2} \text{d}^{-1}$  at 100 m,  
379 and  $90 \pm 20 \mu\text{mol m}^{-2} \text{d}^{-1}$  in the OMZ core at 400 m. These fluxes are equivalent to amino  
380 acid related fluxes of  $16.8 \pm 2.6 \text{ mg C m}^{-2} \text{d}^{-1}$  (100 m) and  $4.48 \pm 1.0 \text{ mg C m}^{-2} \text{d}^{-1}$  (400 m),  
381 respectively, which are typical values for PHAA-C fluxes in the ocean (Lee and Cronin,  
382 1984). PHAA fluxes decreased slightly within the OMZ, i.e. from 300 to 500 m.

383

384

### 385 3.2. Flux attenuation in the ETNA OMZ

386 Fluxes from both deployments were fitted to the exponential decrease model (Martin et al.,  
387 1987) and attenuation coefficients (*b*-values) were estimated for all components (table 1).  
388 Higher *b*-values suggest stronger attenuation and may hint to faster degradation of more labile  
389 components. Accordingly, PHAA were the most labile components of sinking particles during



390 this study, followed by POP, PN, POC, Chl *a*, and TEP (table 1). Attenuation of mineral  
391 fluxes was less pronounced than for TPM.

392 Attenuation coefficient of POC export fluxes was 0.80 during the first and 0.74 during the  
393 second deployment. These values are in the intermediate range of previously determined *b*-  
394 values for POC attenuation in the mesopelagic, shown to vary between 0.51 as determined in  
395 the North Pacific (K2) and 1.59 as determined for the NASG (Buesseler et al., 2007; Marsay  
396 et al., 2015). Based on trap data from fully oxygenated water columns, Marsay et al. (2015)  
397 recently suggested a linear relationship between POC flux attenuation and median water  
398 temperature within the upper 500m of the water column according to:  $b=0.062T+0.303$ .  
399 Applying this relationship to our study area, with temperature decreasing from 26°C at the  
400 surface to 9°C at 500 m and a median temperature value of 12.01°C, would give a *b*-value of  
401 1.05. This estimated *b*-value is higher than the values observed in this study (0.74 - 0.80) and  
402 suggests that oxygen deficiency may reduce attenuation of POC fluxes in the ETNA resulting  
403 in higher  $T_{\text{eff}}$  of organic matter though the OMZ's compared to well oxygenated waters.

404

405 Differences in flux attenuation coefficients translate into different  $T_{\text{eff}}$  for individual  
406 components, with PHAA being the least and TEP being the most efficiently exported organic  
407 component (table 1). In particular, values of  $T_{\text{eff}}$  for TEP and therewith for TEP-C were about  
408 three times higher than for PHAA-C and even clearly higher than for bulk POC, suggesting a  
409 preferential export of carbon included in TEP below 100 m. However, a steep decrease of  
410 TEP flux was observed between 60 m and 100 m during the first deployment. TEP are  
411 produced by a variety of organisms, i.e. different phytoplankton and bacterial species and  
412 cannot be considered as of homogenous composition. Several mechanisms may therefore be  
413 responsible for a change in TEP transfer efficiency with depth: 1) change of TEP  
414 degradability with depth, 2) differences in TEP composition over depth related to association  
415 with particles of different settling speed, 3) new production of TEP, abiotically or by bacteria,



416 during solubilization and degradation of sinking particles, 4) capture of suspended TEP by  
417 sinking aggregates, or 5) reduced degradation rate of TEP at lower oxygen. In support of the  
418 latter hypothesis, an attenuation of TEP fluxes within the OMZ (300-500 m) was not  
419 detectable, but occurred again below the OMZ.

420

### 421 3.3. Changes in POM composition during export

422 POM, assumed to be  $2.2 \times [\text{POC}]$  following Klaas and Archer (2002) made the greatest  
423 contribution to TPM flux at 60 m, but decreased below. Conversely, [%ballast<sub>total</sub>] increased  
424 with depth, namely from 30% w/w at 60 m to 68% w/w at 600 m.

425 Biogenic opal (density:  $2.1 \text{ g cm}^{-3}$ ) in the ocean is produced mainly by diatoms and  
426 radiolarians. During this study, opal made a rather constant contribution to TPM fluxes with  
427 20-25% weight below 100 m. Hence, the observed increase in the [%ballast<sub>total</sub>] with depth  
428 was due to an increasing contribution of  $\text{CaCO}_3$  and lithogenic material. [ $\text{CaCO}_3$ + lith] to  
429 TPM increased from 10-15% above 150 m to 45% at 600 m. As a consequence, the ballast  
430 ratio, defined as [Opal]:[ $\text{CaCO}_3$ +lith] changed from a dominance of opal above the OMZ to a  
431 dominance [ $\text{CaCO}_3$ +lith] within and below the OMZ (Figure 4). Slight differences were  
432 observed between the two deployments. Contribution of Opal and of [ $\text{CaCO}_3$ +lith] to TPM at  
433 100m was almost equal during the first deployment with a share of 18% and 22%,  
434 respectively. During the second deployment the contribution of opal to TPM at 100 m was  
435 21% but only 6% for [ $\text{CaCO}_3$ +lith]. Thus, the higher contribution of opal to TPM fluxes  
436 together with higher Chl *a* fluxes indicated that diatomaceous material had a higher share of  
437 particles sinking out of the euphotic zone down to the OMZ core during the second compared  
438 to the first deployment.

439

440 Molar [POC]:[PN] ratios were close to the Redfield ratio at depths shallower than 100 m,  
441 increased to a ratio of 10 at 400 m depth and remained constant between 400 and 600 m



442 depth (Fig. 5a). [PN]:[POP] ratios were much above Redfield, with values varying between  
443 30 and 45 throughout the water column (Fig. 5b). Also [POC]:[POP] ratios were much higher  
444 than Redfield ratios, and showed an increasing trend down to 300-400 m depth, while  
445 decreasing below (Fig. 5c). These changes in elemental ratios suggested a preferential  
446 remineralization of POP in the upper 300 m, followed by PN and POC deeper down.

447 The percentage of total organic matter in TPM fluxes decreased from 67% at 100m to 32% at  
448 600m (Fig. 6d). As a consequence of higher  $T_{\text{eff}}$  of TEP relative to bulk POC, contribution of  
449 TEP-C to POC increased significantly with depth during both deployments ( $p < 0.01$ ;  $r^2 = 0.59$ ,  
450  $n = 15$ ) and was 2% at 100 m, and 6% within and 5% below the OMZ (Fig. 5e). Because TEP  
451 do not sink by themselves their export to depth depends on their incorporation into settling  
452 aggregates. In a laboratory study, Engel et al. (2009) observed that decomposition of TEP was  
453 faster relative to bulk POC for aggregates formed from calcifying and non-calcifying  
454 *Emiliania huxleyi* cultures. In that experiment, aggregate decomposition was investigated  
455 under oxic conditions. Other studies also showed fast microbial degradation of TEP under  
456 oxic conditions (Bar-Zeev and Rahav, 2015). One possible explanation for increasing [TEP-  
457 C]:[POC] in the hypoxic OMZ of the ETNA region could be that TEP are mostly included in  
458 sinking aggregates, whereas POC could be included in various particle types, such as large  
459 cells, detritus or fecal pellets. Ploug et al. (1997) estimated that carbon turn-over time inside  
460 anoxic aggregates can be strongly reduced. Due to high microbial activity and reduced water  
461 exchange aggregates sinking into hypoxic waters are more likely to experience anoxic  
462 conditions than individual particles (Ploug and Bergkvist, 2015). Thus, TEP settling into  
463 hypoxic waters by aggregates may be exposed to anoxia, and therewith to reduced microbial  
464 degradation, in consequence leading to a preferential TEP transfer through the OMZ. This  
465 may also explain the observed decrease of [TEP-C]:[POC] ratios below the OMZ at 600 m  
466 water depth. Since PN was more rapidly degraded than POC this also implied that the ratio of  
467 [PN]:[TEP-C] became lower with depth.



468

469 In contrast to [TEP-C]:[POC], values of [PHAA-C]:[POC] in POM fluxes declined during  
470 both deployments above the OMZ. However, in the core of the OMZ, at 400 m, [PHAA-  
471 C]:[POC] was higher than at 300 and 500 m (Fig. 5f); the same pattern was also observed  
472 for [PHAA-N]:[PN] (data not shown). A faster decline in PHAA in sinking particles mainly  
473 above but not within the OMZ is different to observations gained for more extensively  
474 oxygen-deficient to full anoxic waters of the Eastern Tropical south Pacific (ETSP), which  
475 suggested that PHAA are preferentially degraded under low oxygen conditions (Van Mooy et  
476 al., 2002). In those studies, total hydrolysable amino acid (THAA) degradation under anoxic  
477 conditions was found to continue with the same rate compared to oxic conditions, while  
478 degradation of non-amino acid compounds was found to slow down (Pantoja et al., 2004; Van  
479 Mooy et al., 2002). A preferential degradation of nitrogen-rich compounds over POC suggests  
480 that microbes degrading organic matter under strongly oxygen deficient conditions via  
481 denitrification preferentially utilize nitrogen-rich amino acids (Van Mooy et al., 2002). Our  
482 data on PHAA do not suggest preferential amino acid loss due to components of sinking POM  
483 degradation in the ETNA OMZ. This is in accordance with the absence of microbial N-loss  
484 processes/ absence of denitrifying bacteria in ETNA oxygen deficient waters (Löscher et al.,  
485 2016). Instead, a slight increase of [PHAA-C]:[POC] in the OMZ may point to higher protein  
486 production by bacterial growth as previously observed for mesopelagic waters (Lee and  
487 Cronin, 1982, 1984) and may be related to increased growth efficiency of bacteria  
488 experiencing low oxygen condition as suggested by Keil et al. (2016).

489

490 Among all amino acids determined, GIX, Gly, Gaba and Leu showed the most pronounced  
491 variations with depth (Fig. 6a-d, table 2). Whereas GIX and Leu showed a decrease with  
492 depth (Fig. 6a, c), Gly continuously increased. It has been shown that Gly is enriched in the  
493 silica-protein complex of diatom frustules (Hecky et al., 1973). Preservation of frustules



494 relative to POM may therefore explain relative increase of Gly with depth in sinking particles.  
495 GIX has been used as a biomarker (Abramson et al., 2010), since GIX was shown to be  
496 enriched in calcereous plankton (Weiner and Erez, 1984). During this study %Mol of GIX was  
497 higher during the first deployment, which is in accordance with the observed higher  
498 contribution of [CaCO<sub>3</sub>+lith] to TPM flux. Gaba has been used as an indicator for bacterial  
499 decomposition activity (Lee and Cronin, 1982; Dauwe and Middelburg, 1998; Engel et al.,  
500 2009). During this study %Mol Gaba behaved differently during the first compared to the  
501 second deployment with similar values within the OMZ, a pattern also observed for opal  
502 fluxes (Fig. 3b). Moreover, %Mol of Gaba showed a local peak at 300 m, i.e. within the  
503 upper oxycline, and may point to high bacterial activity at this depth. Leu is an essential  
504 amino acids and readily taken up by heterotrophic microorganisms. Little change in %Leu in  
505 the OMZ core (Fig. 3d) compared to above (<300 m) indicated reduced microbial reworking  
506 of organic matter under hypoxic conditions. Another indication of microbial reworking of  
507 organic matter can be derived from the Degradation index (DI) (Dauwe et al., 1999). During  
508 this study, the DI decreased with increasing depth, but with differences between the  
509 deployments (Fig. 7). During #2, DI was slightly higher above the OMZ indicating fresher  
510 material. During #1 DI did not decrease within the OMZ, but it continued to decrease from  
511 300 m to 500 m depth during deployment #2. Together with observations on Chl *a* and opal  
512 fluxes, as well as changes in ballast ratio, data on DI suggest that the particles of more  
513 diatomaceous origin likely continued to decompose under hypoxic conditions.

514

515

#### 516 4. Conclusions

517 Despite an improvement in understanding principle processes and drivers of particle export  
518 processes over the past decades, spatial and temporal variability of export fluxes in the ocean  
519 are still difficult to predict. This is partly due to the lack of observations in different regions



520 of the mesopelagic realm. Our study is the first to describe fluxes of POM in the hypoxic  
521 mesopelagic waters of the ETNA. Our data suggest a higher transfer efficiency than expected  
522 from seawater temperature solely, suggesting reduced degradation of organic matter by  
523 heterotrophic communities at low oxygen concentration ( $<60 \mu\text{mol O}_2 \text{ kg}^{-1}$ ). The biological  
524 carbon pump in high productivity regimes associated to OMZs, i.e. Eastern Boundary  
525 Upwelling Systems such as the ETNA region off Mauretania, may therewith be more efficient  
526 than in fully oxygenated waters of comparable temperature. In contrast to suboxic systems ( $<$   
527  $5 \mu\text{mol O}_2 \text{ kg}^{-1}$ ) a relatively higher loss of amino acids from POM fluxes was not evident for  
528 the hypoxic water-column, suggesting microbial N-loss processes were comparatively minor  
529 within particles. This, however, requires further investigation since no corresponding rate  
530 measurements of denitrification or anammox were conducted during this study. Organic  
531 matter composition seems to have a large impact on transfer efficiencies as carbon fluxes  
532 associated to amino acids were much more attenuated over depth than carbon fluxes  
533 associated to polysaccharide-rich TEP. If these findings are transferable to other oceanic  
534 regions, changes in surface ocean organic matter composition in response to climate change  
535 may also impact the carbon remineralization depth and therewith may have a feed-back  
536 potential to atmospheric  $\text{CO}_2$  concentration that yet has to be assessed.

537

### 538 **5. Competing interest**

539 The authors declare that they have no conflict of interest.

540

### 541 **6. Acknowledgements**

542 This study is a contribution to the Collaborative Research Center 754 / SFB

543 Sonderforschungsbereich 754 'Climate-Biogeochemistry Interactions in the Tropical Ocean'.

544 We thank Martin Visbeck, Toste Tanhua, Tobias Hahn, Sunke Schmidtke, and Gerd

545 Krahnmann for scientific and technical support as well as for providing oxygen and CTD data.



546 Many thanks go to the shipboard scientific party and crew of Meteor cruise M105. Jon Roa,  
547 Ruth Flerus, Scarlett Sett and Tania Klüver are acknowledged for technical assistance. We  
548 thank Cindy Lee (Stony Brook University) for helpful advices. FACLM is supported by the  
549 DFG Excellence cluster Future Ocean. All data will become available at [www.pangea.de](http://www.pangea.de)  
550 upon publication.  
551  
552



553 **References**

554

555 Abramson, L., Lee, C., Liu, Z.F., Wakeham, S.G., and Szlosek, J.: Exchange between  
556 suspended and sinking particles in the northwest Mediterranean as inferred from the organic  
557 composition of in situ pump and sediment trap samples. *Limnol. Oceanogr.*, 55, 2, 725-739,  
558 doi: 10.4319/lo.2009.55.2.0725, 2010.

559

560 Alldredge, A. L. and Cohen, Y.: Can microscale chemical patches persist in the sea?  
561 Microelectrode study of marine snow, fecal pellets. *Science*, 235, 4789, 689-91, 1987.

562

563 Alldredge, A. L., and Gotschalk, C. C.: Direct observation of the mass flocculation of diatom  
564 blooms: characteristics, settling velocities and formation of diatom aggregates. *Deep-Sea*  
565 *Research*, 36, 159–171, 1989.

566

567 Alldredge, A. L., U. Passow, and Logan, B. E.: The abundance and significance of a class of  
568 large, transparent organic particles in the ocean. *Deep-Sea Res.* 40, 1131–1140, 1993.

569

570 Arrigo, K. R.: Carbon cycle - Marine manipulations. *NATURE*, 450, 7169, 491-492, 2007.

571

572 Azetsu-Scott, K., and Passow, U.: Ascending marine particles: Significance of transparent  
573 exopolymer particles (TEP) in the upper ocean. *Limnol. Oceanogr.* 49, 3, 741-748, 2004.

574

575 Bar-Zeev, E., and Rahav, E.: Microbial metabolism of transparent exopolymer particles  
576 during the summer months along a eutrophic estuary system. *Frontiers in Microbiol.* 6, 403,  
577 doi: 10.3389/fmicb.2015.00403, 2015.

578



579

580 Belcher, A., Iversen, M., Manno, C., Henson, S. A., Tarling, G. A., and Sanders, R.: The role  
581 of particle associated microbes in remineralization of fecal pellets in the upper mesopelagic of  
582 the Scotia Sea, Antarctica. *Limnol. Oceanogr.* 61, 3, 1049-1064, doi: 10.1002/lno.10269 ,  
583 2016

584

585 Bishop, J. K. B., Ketten, D. K., and Edmon, J. M.: The chemistry, biology and vertical flux of  
586 particulate organic matter from the upper 400 m of the Cape Basin in the southeast Atlantic  
587 Ocean. *Deep-Sea Res.* 25, 1121-1161, 1978.

588

589 Buesseler, K. O.: The decoupling of production and particulate export in the surface ocean.  
590 *Global Biogeochem. Cycles* 12:297-310, 1998.

591

592 Buesseler, K.O., C.H. Lamborg, P.W. Boyd, P.J. Lam, T.W. Trull, R.R. Bidigare, J.K.B.  
593 Bishop, K.L. Casciotti, F. Dehairs, M. Elskens, M. Honda, D.M. Karl, D.A. Siegel, M.W.  
594 Silver, D.K. Steinberg, J. Valdes, B. Van Mooy, and Wilson S.: Revisiting carbon flux  
595 through the ocean's twilight zone. *Science*, 316, 567–570, 2007

596

597 Buesseler, K.O., Antia, A., Chen, M., Fowler, S. W., Gardner, W.D., Gustafsson, O., Harada,  
598 K., Michaels, A.F., van der Loeff, M. R., Sarin, M., Steinberg, D. K. and Trull, T.: An  
599 assessment of the use of sediment traps for estimating upper ocean particle fluxes *Journal of*  
600 *Marine Research*, 65, 345-416, 2007.

601

602 Buesseler, K.O., and Boyd P.W.: Shedding light on processes that control particle export and  
603 flux attenuation in the twilight zone, *Limnol. Oceanogr.*, 54, 4, 1210–1232, 2009

604



- 605 Cavan, E.L., Le Moigne, F. A. C., Poulton, A. J., Tarling, G. A., Ward, P., Daniels, C. J.,  
606 Fragoso, G. M., and Sanders, R. J. : Attenuation of particulate organic carbon flux in the  
607 Scotia Sea, Southern Ocean, is controlled by zooplankton fecal pellets. *Geophys. Res. Lett.*,  
608 42, 3, 821-830, doi: 10.1002/2014GL062744, 2015
- 609
- 610 Chow, J. S., Lee, C. and Engel, A.: The influence of extracellular polysaccharides, growth  
611 rate, and free coccoliths on the coagulation efficiency of *Emiliana huxleyi*. *Mar. Chem.*, 175,  
612 2015.
- 613
- 614 Dauwe, B., and Middelburg, J.J.: Amino acids and hexosamines as indicators of organic  
615 matter degradation state in North Sea sediments. *Limnol. Oceanogr.* 43, 782-798, 1998.
- 616
- 617 Dauwe, B., Middelburg, J. J., Herman, P. M. J., and Heip, C. H. R.: Linking diagenetic  
618 alteration of amino acids and bulk organic matter reactivity. *Limnol. Oceanogr.* 44, 1809–  
619 1814, 1999.
- 620
- 621 Devol, A.H. and Hartnett, H. E.: Role of the oxygen minimum zone in transfer of organic  
622 carbon to the deep ocean. *Limnol. Oceanogr.*, 25, 1684-1690, 2001.
- 623
- 624 Ebersbach, F., Assmy, P., Martin, P. et al.: Particle flux characterisation and sedimentation  
625 patterns of protistan plankton during the iron fertilisation experiment LOHAFEX in the  
626 Southern Ocean. *Deep Sea Res. I*, 89, 94-103, 2014.
- 627
- 628 Engel, A.: The role of transparent exopolymer particles (TEP) in the increase in apparent  
629 particle stickiness ( $\alpha$ ) during the decline of a diatom bloom. *J. Plankton Res.*, 22, 485-  
630 497, 2000.



631

632 Engel, A. und Passow, U.: Carbon and nitrogen content of transparent exopolymer particles  
633 (TEP) in relation to their Alcian Blue adsorption. Mar. Ecol. Prog. Ser., 219, 1-10,  
634 doi:10.3354/meps219001, 2001.

635

636 Engel, A., Thoms, S., Riebesell, U., Rochelle-Newall, E. and Zondervan, I.: Polysaccharide  
637 aggregation as a potential sink of marine dissolved organic carbon. Nature, 428, 929-932,  
638 2004.

639

640 Engel, A., Abramson, L., Szlosek, J., Liu, Z., Stewart, G., Hirschberg, D. and Lee, C.:  
641 Investigating the effect of ballasting by CaCO<sub>3</sub> in *Emiliana huxleyi*, II: Decomposition of  
642 particulate organic matter. Deep-Sea Res. II, 56, 18, 1408-1419. DOI  
643 10.1016/j.dsr2.2008.11.028, 2009.

644

645 Engel, A.: Determination of Marine Gel Particles, in: Practical Guidelines for the Analysis of  
646 Seawater, edited, CRC Press, 2009.

647

648 Engel, A., Piontek, J., Grossart, H. P., Riebesell, U., Schulz, K. G. and Sperling, M.: Impact  
649 of CO<sub>2</sub> enrichment on organic matter dynamics during nutrient induced coastal phytoplankton  
650 blooms. J Plankton Res., 36, 3, 641-657. DOI 10.1093/plankt/fbt125, 2014.

651

652 Sarah L. C. Giering, S. L. C., Sanders, R., Lampitt, R. S., Anderson, T. A., Tamburini, C.,  
653 Boutrif, M., Zubkov, M. V., Marsay, C. M., Henson, S. A., Saw, K., Cook, K., and Mayor,  
654 D. J. Reconciliation of the carbon budget in the ocean's twilight zone. Nature, 507, 480-483,  
655 2014.

656



- 657 Haake, B., Ittekkot, V., Ramaswamy, V., Nair, R. R., and Honjo, S. Fluxes of amino acids  
658 and hexosamines to the deep Arabian Sea, *Mar. Chem.*, 40, 291–314, 1992.
- 659
- 660 Hansen, H.P, and Koroleff, F.: Determination of nutrients. In: *Methods of seawater analysis*.  
661 Grasshof, K. (ed), 159–228, 1999.
- 662
- 663 Hecky, R.E., Mopper, K., Kilham, P., and Degens, E. T.: Amino acid and sugar composition  
664 of diatom cell-walls. *Mar. Biol.*, 19, 4, 323-331, doi: 10.1007/BF00348902, 1973.
- 665
- 666 Heinze, C., Meyer, S., Goris, N., Anderson, L., Steinfeldt, R., Chang, N., Le Quere, C., and  
667 Bakker, D. C. E. : The ocean carbon sink - impacts, vulnerabilities and challenges. *Earth Syst*.  
668 *Dynamics*, 6, 1, 327-358, doi: 10.5194/esd-6-327-2015, 2015.
- 669
- 670 Iversen, M. H., Nowald, N., Ploug, H., Jackson, G. A., and Fischer, G.: High resolution  
671 profiles of vertical particulate organic matter export off Cape Blanc, Mauritania: Degradation  
672 processes and ballasting effects. *Deep-Sea Res.*, 57, 6, 771-784,  
673 doi:10.1016/j.dsr.2010.03.007, 2010.
- 674
- 675 Karstensen, J., Stramma, L., and Visbeck, M. (2008) Oxygen minimum zones in the eastern  
676 tropical Atlantic and Pacific oceans, *Prog. Oceanogr.*, 77, 331–350.
- 677
- 678 Keil, R. G., Neibauer, J., Biladeau, C., van der Elst, K. and Devol A. H.: A multiproxy  
679 approach to understanding the “enhanced” flux of organic matter through the oxygen deficient  
680 waters of the Arabian Sea. *Biogeosciences*, 13, 2077-2092, 2015.
- 681
- 682 Klaas, C., and Archer, D. E.: Association of sinking organic matter with various types of



683 mineral ballast in the deep sea: Implications for the rain ratio. *Global Biogeochem. Cycles*,  
684 16(4), 1116, doi:10.1029/2001GB001765, 2002.

685

686 Knauer, G.A., J.H. Martin, and Bruland, K.W.: Fluxes of particulate carbon, nitrogen, and  
687 phosphorus in the upper water column of the northeast Pacific. *Deep-Sea Research*, 26, 97-  
688 108, 1979.

689

690 Kohlfeld, K. E., and Ridgwell, A. Glacial-Interglacial Variability in Atmospheric CO<sub>2</sub>. In:  
691 *Surface Ocean–Lower Atmosphere Processes Geophysical Research Series*, 187, American  
692 Geophysical Union, doi:10.1029/2008GM000845, 2009.

693

694 Kwon, E. Y., Primeau, F., and Sarmiento J. L.: The impact of remineralization on the air-sea  
695 carbon balance, *Nat. Geosci.*, 2, doi:10.1038/ngeo612, 2009.

696

697 Lam, P. J, Doney, S. C. and Bishop J. K. B.: The dynamic ocean biological pump: Insights  
698 from a global compilation of particulate organic carbon, CaCO<sub>3</sub> and opal concentrations  
699 profiles from the mesopelagic. *Global Biogeochem. Cycles.*, 25, GB3009, doi:  
700 10.1029/2010GB003868, 2011.

701

702 Lampitt, R. S., Noji, T. and Von Bodungen, B.: What happens to zooplankton fecal pellets-  
703 implications for material flux. *Mar. Biol.*, 104, 1, 15-23, doi: 10.1007/BF01313152, 1990.

704

705 Le Moigne, F. A. C., Henson, S. A., Cavan, E., Georges, C., Pabortsava, K., Achterberg, E.P.,  
706 Ceballos-Romero, E., Zubkov, M. and Sanders, R. J.: What causes the inverse relationship  
707 between primary production and export efficiency in the Southern Ocean?, *Geophys. Res.*  
708 *Let.*, doi:10.1002/2016GL068480, 2016.



709

710 Lee, C., and Cronin, C.: The vertical flux of particulate nitrogen in the sea: Decomposition of  
711 amino acids in the Peru upwelling area and the equatorial Atlantic. *J. Mar. Res.* 40, 227-251,  
712 1982.

713

714 Lee, C., and Cronin, C., Particulate amino acids in the sea: Effects of primary productivity  
715 and biological decomposition. *Journal of Marine Research* 42, 1075-1097, 1984.

716

717 Lindroth, P., and Mopper, K.: High performance liquid chromatographic determination of  
718 subpicomole amounts of amino acids by precolumn fluorescence derivatization with o-  
719 phthaldialdehyde, *Analytical Chemistry*, 51(11), 1667-1674, 1979.

720

721 Löscher, C., Bange, H. W., Schmitz, R. A., Callbeck, C. M., Engel, A., Hauss, H., Kanzow,  
722 T., Kiko, R., Lavik, G., Loginova, A. N., Melzner, F., Meyer, J., Neulinger, S. C., Pahlow,  
723 M., Riebesell, U., Schunck, H., Thomsen, S. and Wagner, H.: Water column biogeochemistry  
724 of oxygen minimum zones in the eastern tropical North Atlantic and eastern tropical South  
725 Pacific Oceans. *Biogeosciences (BG)*, 13 . pp. 3585-3606. DOI 10.5194/bg-13-3585-2016,  
726 2016.

727

728 Mari, X.: Carbon content and C:N ratio of transparent exopolymeric particles (TEP) produced  
729 by bubbling exudates of diatoms. *Mar. Ecol. Progr. Ser.*, 183, 59-71, 1999.

730

731 Marsay, C. M., Sanders, R. J., Henson, S. S., Pabortsava, K., Achterberg, E. P., and Lampitt,  
732 R. S.: Attenuation of sinking particulate organic carbon flux through the mesopelagic ocean.  
733 *Proc. Natl. Acad. Sci. U.S.A.*, 112, 4, 1089-1094, doi: 10.1073/pnas.1415311112, 2015.

734



735 Martin, P., Lampitt, R. S., Perry, M. J. Sanders, R. Lee, C., and D'Asaro, E.: Export and  
736 mesopelagic particle flux during a North Atlantic spring diatom bloom. *Deep-Sea Research I*  
737 58, 338–349, 2011.

738

739 Martin, J.H., G.A. Knauer, D.M. Karl and Broenkow W.W.: Vertex – Carbon Cycling in the  
740 Northeast Pacific. *Deep-Sea Res. A*, 34, 267-285, doi: 10.1016/0198-0149(87)90086-0, 1987.

741

742 Mortlock, R.A., and Froelich, P.N.: A simple method for the rapid determina- tion of biogenic  
743 opal in pelagic marine sediments. *Deep-Sea Res., Part A*, 36, 1415– 1426, 1989.

744

745 Pantoja, S., Sepúlveda, J. and González H. E.: Decomposition of sinking proteinaceous  
746 material during fall in the oxygen minimum zone off northern Chile. *Deep Sea Research, I*,  
747 51, 55-70, 2004.

748

749 Passow, U.: Transparent exopolymer particles (TEP) in aquatic environments, *Progress in*  
750 *Oceanography*, 55, 287-333, 2002.

751

752 Passow, U., Shipe, R. F., Pak, D. K., Brzezinski, M. A., & Alldredge, A. L.: Origin of  
753 transparent exopolymer particles (TEP) and their role in the sedimentation of particulate  
754 matter. *Continental Shelf Research*, 21, 327–346, 2000.

755

756 Ploug, H., Kühl M., Buchholz-Cleven, B., and Jørgensen, B.B.: Anoxic aggregates - an  
757 ephemeral phenomenon in the pelagic environment? *Aquat. Microb. Ecol.*, 13, 285–294,  
758 1997.

759



760 Ploug, H., and B.B. Jørgensen (1999) A net-jet flow system for mass transfer and  
761 microelectrode studies in sinking aggregates. *Mar. Ecol. Prog. Ser.* 176, 279-290.

762

763 Ploug, H., and Bergkvist, J.: Oxygen diffusion limitation and ammonium production within  
764 sinking diatom aggregates under hypoxic and anoxic conditions. *Mar. Chem.* 176, 142-149,  
765 2015.

766

767 Schlitzer, R., Ocean Data View, <http://odv.awi.de>, 2013.

768

769 Schneider, B., Engel, A., and Schlitzer, R.: Effects of depth- and CO<sub>2</sub>-dependent C:N ratios  
770 of particulate organic matter (POM) on the marine carbon cycle. *Global Biogeochemical*  
771 *Cycles*, 18, 2, doi:10.1029/2003GB002184, 2004.

772

773 Soutar, A., Kling, S. A., Crill, P. A., Duffrin, E., and Bruland K.W.: Monitoring the marine  
774 environment through sedimentation. *Nature*, 266, 136-139, 1977.

775

776 Stief, P., Kamp, A., Thamdrup, B., and Glud, R.N. : Anaerobic Nitrogen Turnover by Sinking  
777 Diatom Aggregates at Varying Ambient Oxygen Levels. *Frontiers in Microbiol.*, 7, 98 doi:  
778 10.3389/fmicb.2016.00098, 2016.

779

780 Stramma, L., Johnson, G. C., Sprintall, J., and Mohrholz, V.: Expanding Oxygen-Minimum  
781 Zones in the Tropical Oceans, *Science*, 320, 655-658, 2008.

782

783 Suess, E.: Particulate organic carbon flux in the oceans - surface productivity and oxygen  
784 utilization, *Nature* 288, 260-263, 1980.

785



786 Torres Valdez, S., Painter, . C., Martin, A. P., Sanders, R. and Felden, J.: Data compilation of  
787 fluxes of sedimenting material from sediment traps in the Atlantic Ocean. Earth system  
788 Science Data, 6, 123-145, doi: 10.5194/essd-6-123-2014, 2014.

789

790 Van Mooy, B. A. S., Keil R. G., and Devol, A. H.: Impact of suboxia on sinking particulate  
791 organic carbon: Enhanced carbon flux and preferential degradation of amino acids via  
792 denitrification. Geochim. Cosmochim. Ac., 66, 457-465. doi: 10.1016/s0016-7037(01)00787,  
793 2002.

794

795 Visbeck M.: Oxygen in the Tropical Atlantic OSTRE Second Tracer Survey – Cruise. No.  
796 M105 – March 17 – April 16, 2014 – Mindelo (Cape Verde) – Mindelo (Cape Verde).  
797 METEORBerichte, M105, 49 pp., DFG-Senatskommission für Ozeanographie,  
798 DOI:10.2312/cr\_m105, 2014.

799

800 Volk, T., and Hoffert, M. I.: Ocean carbon pumps: Analysis of relative strengths and  
801 efficiencies in ocean driven atmospheric CO<sub>2</sub> changes. In: Sundquist ET and Broecker WS  
802 (eds.) The Carbon Cycle and Atmospheric CO<sub>2</sub>: Natural Variations Archean to Present,  
803 Geophysical Monograph Series, vol. 32, pp. 99-110. Washington, DC: American Geophysical  
804 Union, 1985.

805

806 Weiner, S. and Erez, J.: Organic matrix of the shell of the foraminifer *Heterostegina*  
807 *depressa*. Journal of Foraminifera Res., 14, 3, 206-212, 1984.

808

809 Welschmeyer, N. A.: Fluometric analysis of chlorophyll a in the resence of chlorophyll b and  
810 pheopigments. Limnol. Oceanogr., 39, 1985-1992, 1994.

811

812 **Tables**

813

814 Table 1: Fluxes of particulate components at 100m depth ( $F_{100}$ ) and in the core of the OMZ at  
 815 400m ( $F_{OMZ}$ ), as well as the associated attenuation coefficients ( $b$ -values) and transfer  
 816 efficiencies ( $T_{eff}$ , %) over the depth range 100 to 600 m during two traps deployments in the  
 817 ETNA. All units are in  $\text{mg m}^{-2} \text{d}^{-1}$  except for TEP fluxes which is reported in total particle  
 818 area  $\text{cm}^{-2} \text{m}^{-2} \text{d}^{-1}$ . Mean values and standard deviations (SD) were calculated from analytical  
 819 replicates.

Component		$F_{100}$		$F_{OMZ}$		$b$ -value		$T_{eff}$ (%)	
		mean	SD	mean	SD	mean	SD	$r^2$	(600/100 m)
Mass	I	249	48.9	141	6.8	-0.429	0.090	0.987	41
	II	231	16.3	141	12.1	-0.355	0.033	0.998	52
POC	I	69.4	9.23	23.8	5.4	-0.795	0.031	0.989	23
	II	76.3	8.43	28.1	3.0	-0.741	0.044	0.989	22
PN	I	11.9	1.29	2.76	0.46	-1.013	0.026	0.992	15
	II	13.5	1.12	3.26	0.19	-1.00	0.020	0.990	16
POP	I	0.71	0.07	0.15	0.02	-1.081	0.074	0.992	18
	II	0.64	0.03	0.22	0.02	-0.80	0.034	0.990	23
Opal	I	44.6	1.76	34.0	1.7	-0.195	0.038	0.987	65
	II	48.6	4.16	30.7	2.0	-0.345	0.052	0.987	44
Chl $a$	I	0.10	0.00	0.035	0.001	-0.820	0.024	0.990	21
	II	0.12	0.01	0.053	0.005	-0.625	0.082	0.988	24
TEP	I	1650	548	119	36.8	-0.498	0.014	0.548	33
	II	2990	348	1644	95	-0.451	0.069	0.810	37
PHAA-C	I	3.21	-	3.71	0.47	-1.324	0.067	0.994	11
	II	1.28	0.10	5.24	0.79	-0.978	0.096	0.991	14

820

821

822



823 Table 2: Composition of PHAA (%Mol) collected at different depths during two trap  
 824 deployments (#I, #II) in the ETNA region.

Depth													
(m)	AsX	GlX	Ser	Gly	Thr	Arg	Ala	GABA	Tyr	Val	Iso	Phe	Leu
#I													
60	14.15	13.94	8.46	14.29	7.76	5.90	11.94	0.22	0.84	5.69	4.57	4.00	8.26
100	13.95	13.53	8.29	14.65	7.87	5.77	11.57	0.19	1.64	5.66	4.56	4.07	8.24
150	14.19	12.73	8.54	15.93	8.10	5.78	11.42	0.31	0.96	5.68	4.44	4.05	7.87
200	14.17	12.05	9.29	16.02	8.05	5.61	11.69	0.49	1.10	5.65	4.30	4.04	7.54
300	13.19	11.75	8.58	17.71	7.98	5.31	12.10	0.37	1.82	5.77	4.15	3.83	7.43
400	14.15	11.77	9.03	18.54	7.94	5.72	10.85	0.46	1.25	5.58	3.93	3.80	6.97
500	14.06	11.89	9.55	18.70	7.18	6.01	11.02	0.55	1.29	5.19	3.86	3.65	7.05
600	14.15	13.94	8.46	14.29	7.76	5.90	11.94	0.22	0.84	5.69	4.57	4.00	8.26
#II													
100	13.89	14.69	8.36	12.94	7.57	5.89	12.26	0.21	0.02	6.13	5.12	4.05	8.86
150	13.48	14.23	8.46	14.12	7.56	5.68	12.55	0.22	0.00	6.21	5.01	3.85	8.62
200	13.80	13.90	9.10	14.27	7.20	6.12	11.57	0.27	0.04	6.19	5.07	3.97	8.49
300	14.58	14.63	8.35	15.16	7.75	5.56	11.75	0.26	0.14	5.62	4.51	3.82	7.88
400	14.06	13.01	8.72	16.45	7.99	5.55	11.74	0.44	0.79	5.54	4.33	3.77	7.59
500	14.08	12.90	8.75	16.48	7.59	5.69	11.81	0.37	0.30	5.94	4.62	3.80	7.66
600	13.62	12.55	9.16	17.02	7.95	5.75	11.23	0.42	0.38	5.87	4.61	3.88	7.55

825

826

827

828

829

830



831 **Figure captions:**

832

833

834 Figure 1a-d: Map of the study area (A) and depth distribution of oxygen concentration (mol  
835  $\text{kg}^{-1}$ ) (B) in the Eastern Tropical North Atlantic (ETNA) during the RV Meteor 105 cruise,  
836 when two surface tethered drifting sediment traps (STDT) were deployed (C). Depth  
837 distribution of oxygen concentration (mol  $\text{kg}^{-1}$ ) at stations visited in the deployment area  
838 showed an oxygen minimum zone in the upper mesopelagial (D).

839

840 Figure 2a-d: Fluxes of total mass (a) and particulate organic carbon (b; POC), particulate  
841 nitrogen (c; PN), and particulate organic phosphorus (d; POP) during the deployment of two  
842 STDT in the ETNA. Deployments: Solid symbols #I, open symbols #II.

843

844 Figure 3a-d: Fluxes of Chlorophyll *a* (a; Chl *a*), opal (b), TEP (c), and PHAA (d) during the  
845 deployment of two STDT in the ETNA. Deployments: Solid symbols #I, open symbols #II.

846

847 Figure 4: Changes in mineral ballast ratios of sinking particles with depth during the two  
848 deployments in the ETNA. Deployments: Black bars #I, grey bars #II.

849

850 Figure 5a-f: Changes in organic matter composition of particles sinking through the OMZ  
851 during the deployment of two STDT in the ETNA. Deployments: Solid symbols #I, open  
852 symbols #II.

853

854 Figure 6a-d: Molar percentages of selected amino acids contained in PHAA during the  
855 deployment of two STDT in the ETNA. Deployments: Solid symbols #I, open symbols #II.

856



857 Figure 7: Degradation index (DI) of organic matter in trap collected sinking particles based on

858 amino acid composition and calculated after Dauwe et al. (1999). Deployments: Black bars

859 #I, grey bars #II.

860

861

862

863

864

865

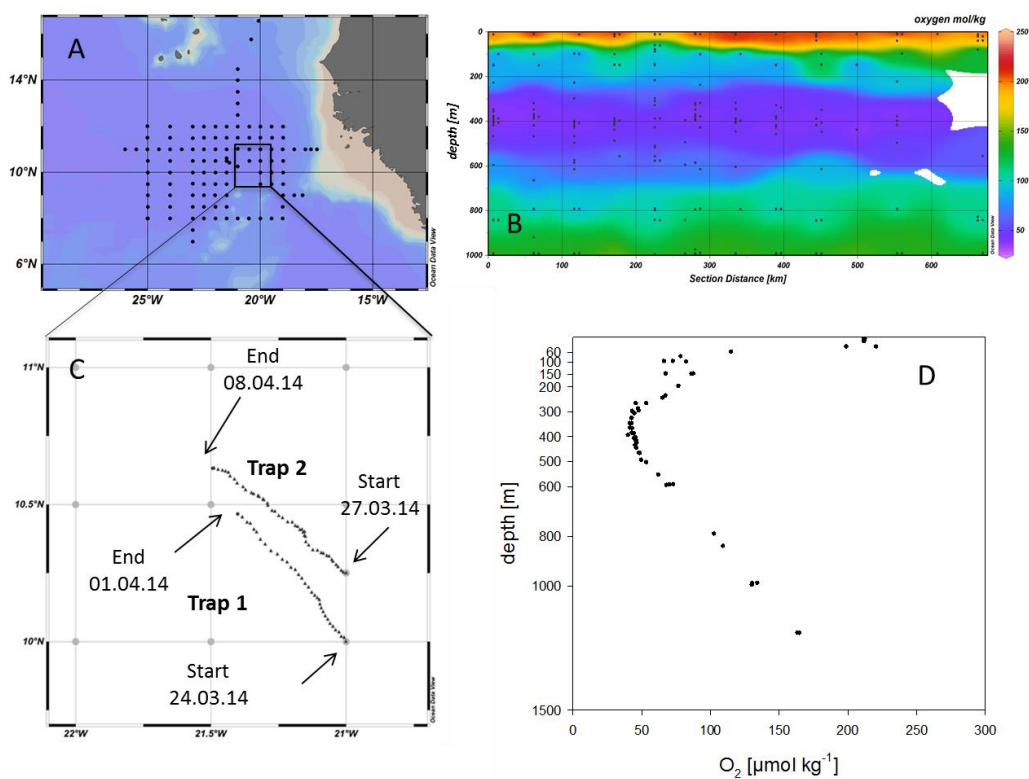


866

867

868 **Figures**

869



870

871

872

873

874

875

Figure 1a-d



876

877

878

879

880

881

882

883

884

885

886

887

888

889

890

891

892

893

894

895

896

897

898

899

900

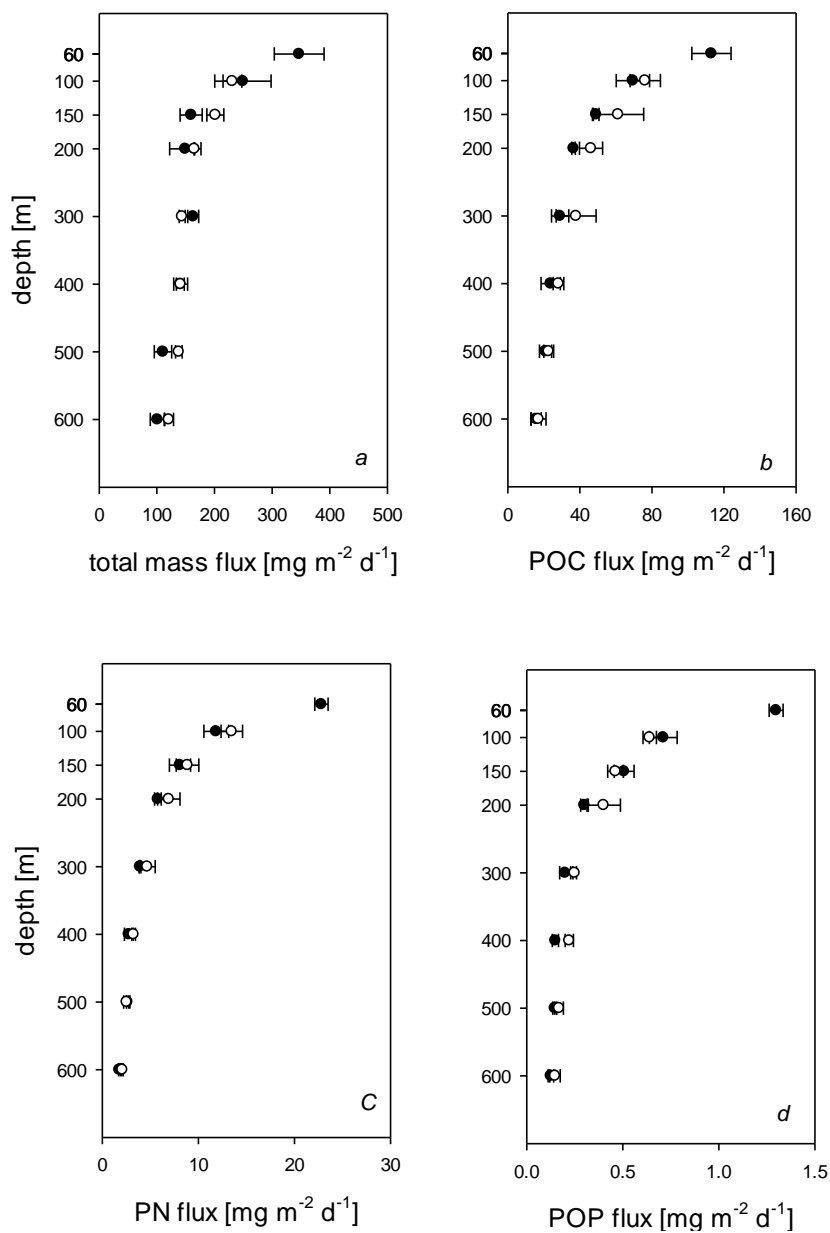
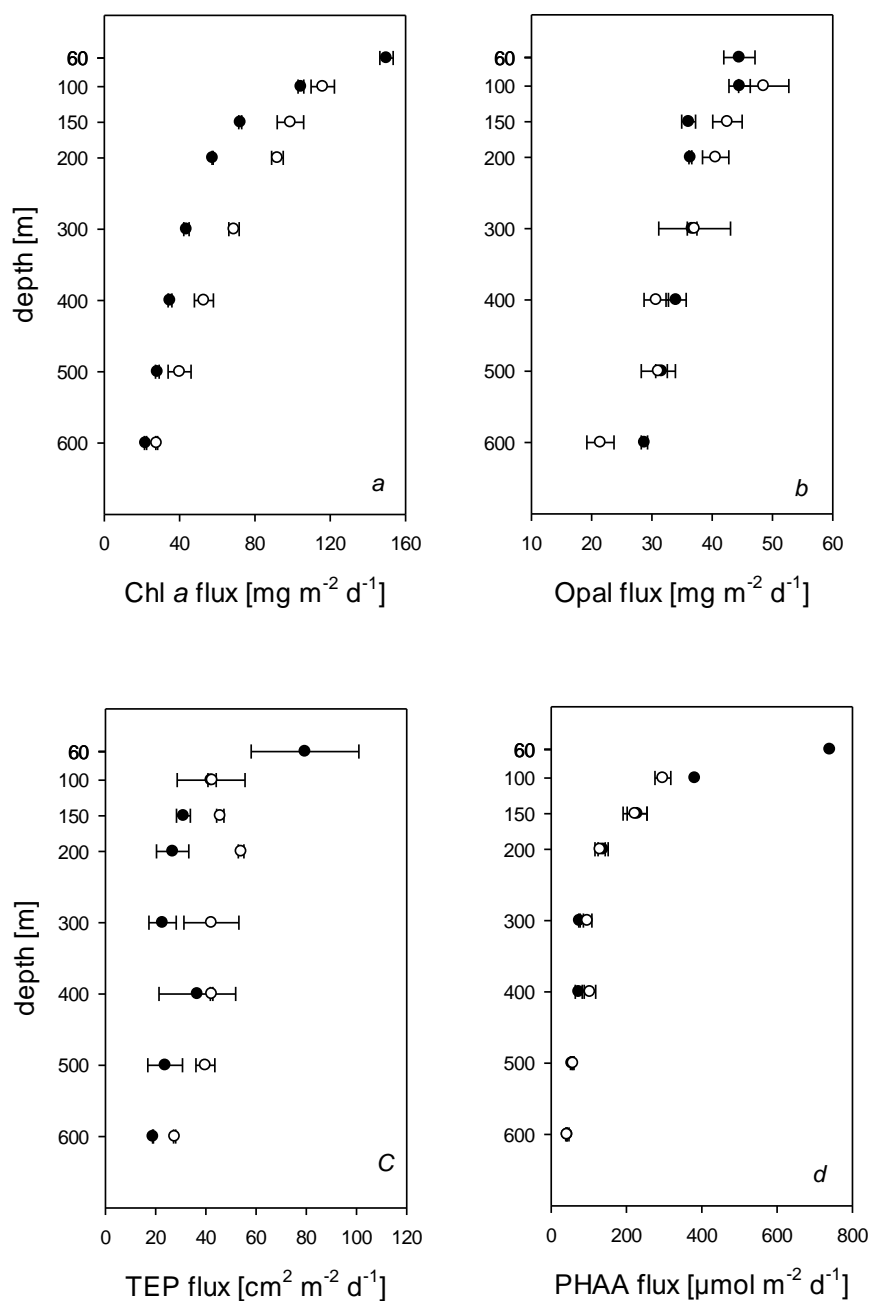


Figure 2a-d



901  
 902  
 903  
 904

Figure 3a-d



905

906

907

908

909

910

911

912

913

914

915

916

917

918

919

920

921

922

923

924

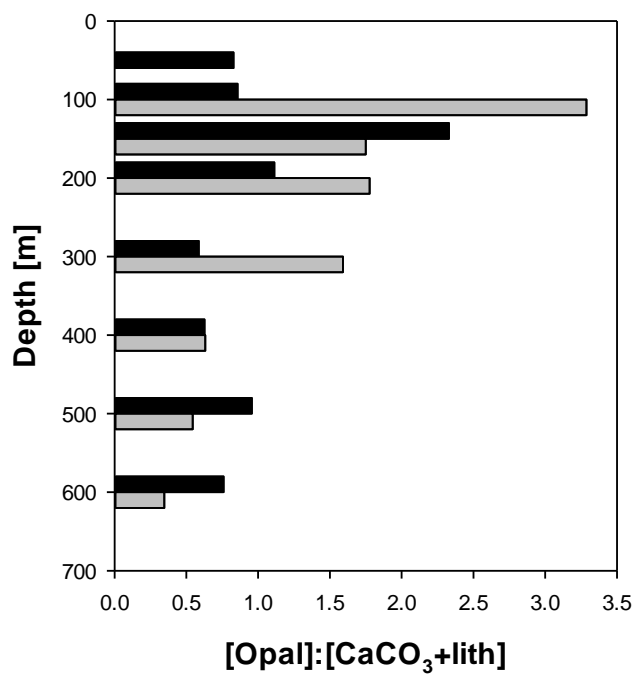
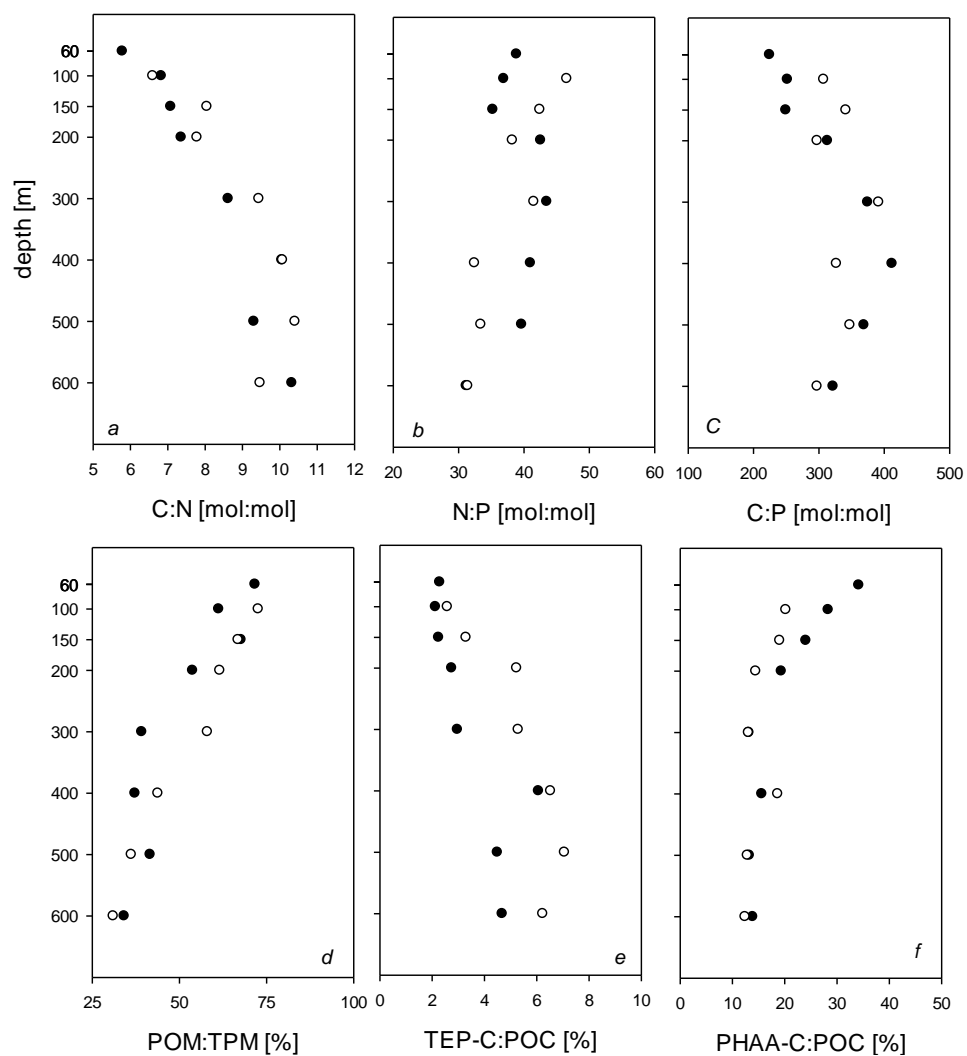


Figure 4



925

926

927

928

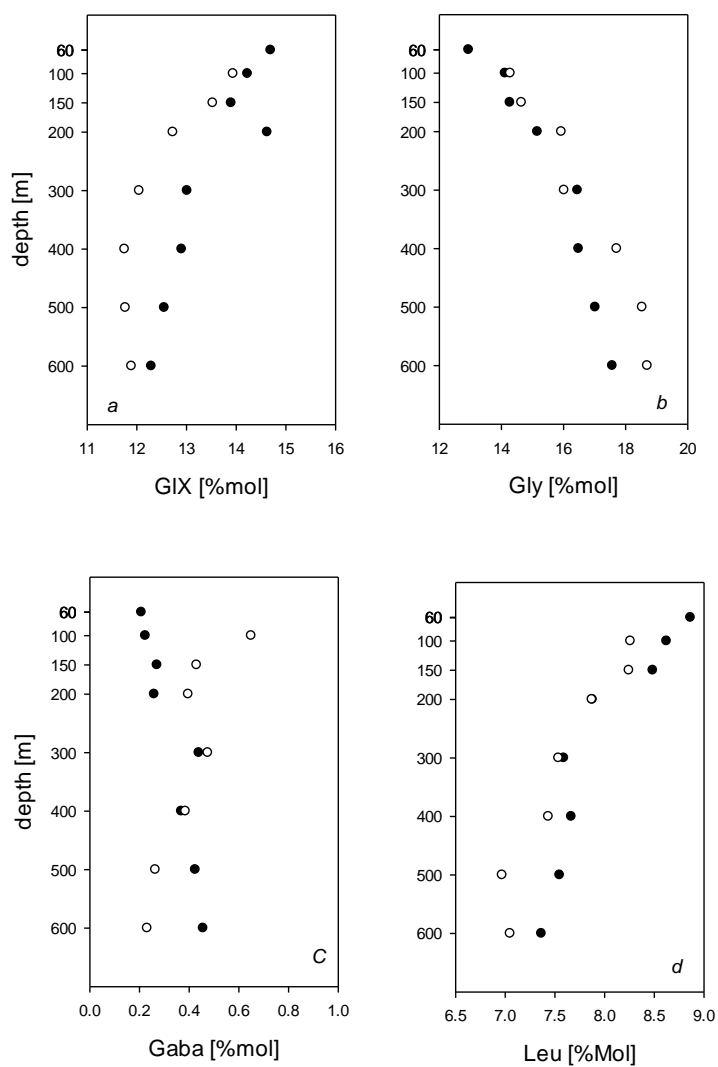
929

930

931

932

Figure 5a-f



933

934

935

936

Figure 6a-d

937

938

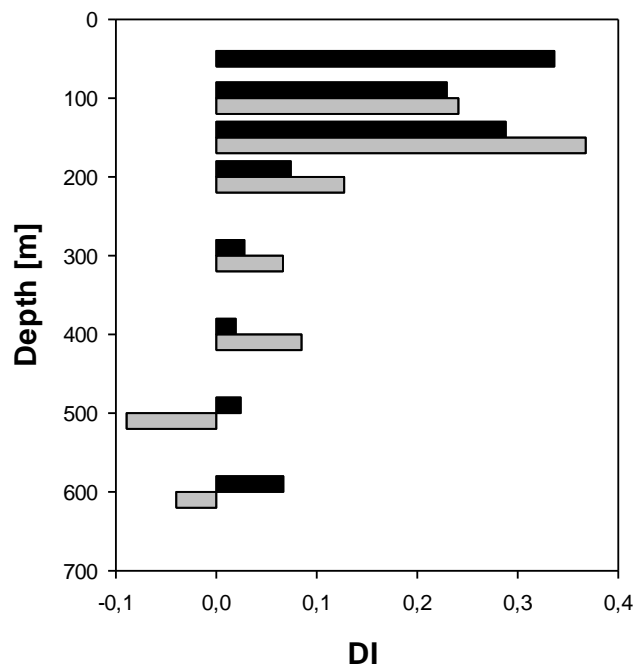
939

940



941

942



943

944

945

Figure 7